THE JOURNAL OF PHYSICAL CHEMISTRY A

Article

pubs.acs.org/JPCA

# Phase Transitions and Phase Miscibility of Mixed Particles of Ammonium Sulfate, Toluene-Derived Secondary Organic Material, and Water

Mackenzie L. Smith,[†] Yuan You,[‡] Mikinori Kuwata,[†] Allan K. Bertram,*[,‡] and Scot T. Martin*[,†,§]

[†]School of Engineering and Applied Sciences and [§]Department of Earth and Planetary Sciences, Harvard University, Cambridge, Massachusetts 02138, United States

[‡]Department of Chemistry, University of British Columbia, Vancouver, British Columbia V6T 1Z1, Canada

Supporting Information

**ABSTRACT:** The phase states of atmospheric particles influence their roles in physicochemical processes related to air quality and climate. The phases of particles containing secondary organic materials (SOMs) are still uncertain, especially for SOMs produced from aromatic precursor gases. In this work, efflorescence and deliquescence phase transitions, as well as phase separation, in particles composed of toluene-derived SOM, ammonium sulfate, and water were studied by hygroscopic tandem differential mobility analysis (HTDMA) and optical microscopy. The SOM was produced in the Harvard Environmental Chamber by photo-oxidation of toluene at chamber relative humidities of <5 and 40%. The efflorescence and deliquescence relative humidities (ERH and DRH, respectively, studied by HTDMA) of ammonium sulfate decreased as the SOM organic fraction $\varepsilon$ in the particle increased, dropping from DRH = 80% and ERH = 31% for $\varepsilon$ = 0.0 to DRH = 58% and ERH = 0% for $\varepsilon$ = 0.8. For $\varepsilon$ < 0.2, the DRH and ERH to first approximation did not change with the organic volume fraction. This observation is consistent with independent behaviors for $\varepsilon$ < 0.2 of water-infused toluene-derived SOM and aqueous ammonium sulfate, suggesting phase immiscibility between the two. Optical microscopy of particles prepared for $\varepsilon$ = 0.12 confirmed phase separation for RH < 85%. For $\varepsilon$ from 0.2 to 0.8, the DRH and ERH values steadily decreased, as studied by HTDMA. This result is consistent with one-phase mixing of ammonium sulfate, SOM, and water. Optical microscopy for particles of $\varepsilon$ = 0.8 confirmed this result. Within error, increased exposure times of the aerosol in the HTDMA from 0.5 to 30 s affected neither the ERH($\varepsilon$) nor DRH($\varepsilon$) curves, implying an absence of kinetic effects on the observations over the studied time scales. For $\varepsilon$ > 0.5, the DRH values of ammonium sulfate in mixtures with SOM produced at <5% RH were offset by −3 to −5% RH compared to the results for SOM produced at 40% RH, suggesting differences in SOM chemistry. The observed miscibility gap (i.e., phase separation) between toluene-derived SOM and aqueous ammonium sulfate across a limited range of organic volume fractions differentiates this SOM from previous reports for isoprene-derived SOM of full miscibility and for $\alpha$-pinene-derived SOM of nearly full immiscibility with aqueous ammonium sulfate.

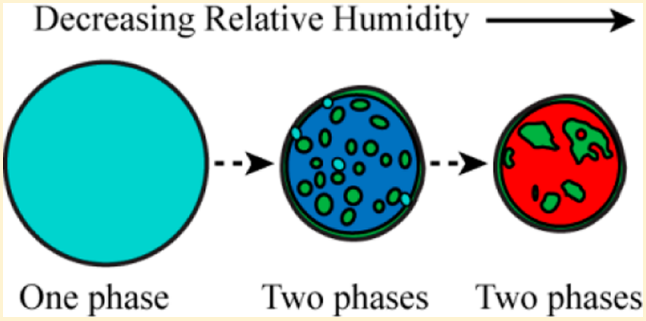


## 1. INTRODUCTION

Atmospheric aerosol particles scatter and absorb radiation, act as ice and cloud condensation nuclei, and take part in heterogeneous processes such as hydrolysis reactions and gas-to-particle partitioning.[1] The participation of particles in these processes is influenced by phase and morphology, which in turn depend on particle composition, relative humidity (RH), and temperature.[2−5] Phase transitions of crystalline inorganic materials commonly found in atmospheric particles, such as sodium chloride and ammonium sulfate, have been significantly studied.[6−8] These materials change from a crystalline solid to a saturated aqueous solution at the deliquescence relative humidity (DRH), defined as the RH at which the Gibb's free energy of a saturated solution droplet is equal to that of the solid surrounded by water vapor.[7] The solution droplet can crystallize back to a solid at the efflorescence relative humidity (ERH) through a mechanism of critical germ formation followed by crystal growth.[8]

In the atmosphere, mixed particles of organic and inorganic components are common.[9−13] Organic molecules in the gas phase can condense onto the surfaces of pre-existing inorganic particles and further grow by absorptive partitioning.[14] Another mechanism for formation of these particles is the uptake and reaction of gas-phase organic molecules in aqueous droplets, leaving behind a mixed particle after cloud evaporation.[15] The phase behavior of the inorganic and organic materials within

Received: May 23, 2013
Revised: August 8, 2013
Published: August 9, 2013

  

Table 1. Summary of the Literature Regarding the Deliquescence and Efflorescence Phase Transitions of Internally Mixed Particles of Ammonium Sulfate, Laboratory-Generated SOM, and Water[a]

| SOM production | RH (%) during production | $M_{org}$ ($\mu$g m$^{-3}$) | O/C | range $\varepsilon_{min}$–$\varepsilon_{max}$ | DRH (%) | ERH (%) |
|---|---|---|---|---|---|---|
| $\beta$-caryophyllene ozonolysis | 40[16] | 17.4 | 0.35 | 0.18–0.96 | 79.5–79.0 | 28.7–28.3 |
| limonene ozonolysis | 6–10[23] | na | na | 0.59–0.94 | na | 28–34 ± 2.5 |
| $\alpha$-pinene ozonolysis | 40[20] | 1.63 | 0.44 | 0.15–0.76 | 80.4–79.7 | 30.0–29.8 |
| | 40[20] | 12.2 | 0.39 | 0.18–0.99 | 79.2–77.3 | 29.7–29.0 |
| | 40[24] | na | 0.30 | 0.67[b] | 77 ± 4 | 35–40 |
| | 6–10[23] | na | na | 0.54–0.72 | na | 28–34 ± 2.5 |
| | 45[25] | na | na | 0.18 | between 70 and 80 | na |
| $\alpha$-pinene photo-oxidation | 50[26] | na | na | 0.0–0.2 | between 75 and 85 | na |
| | | | | 0.2–0.9 | <75 | na |
| isoprene photo-oxidation | 40, 60[18] | 20–30 | 0.67–0.74 | 0.0–0.86 | 80–47.8 | 31–7 |
| $p$-xylene photo-oxidation | 21.8[27] | 6.4 | na | 0.13 | 80 | 30 |
| toluene photo-oxidation | 25.7[27] | 8.2 | na | 0.16 | 80 | 30 |
| 1,3,5-trimethylbenzene photo-oxidation | 28.0[27] | 2.0 | na | 0.05 | 80 | 30 |
| 1,2,4-trimethylbenzene photo-oxidation | 18[24] | na | 0.4 | 0.8 | na | 35–40 |

[a]The DRH and ERH of pure ammonium sulfate are 79.5 and 30–35%, respectively.[7] [b]The org/sulf mass ratio was converted to the organic volume fraction $\varepsilon$ using material densities of 1770 kg m$^{-3}$ for ammonium sulfate and 1200 kg m$^{-3}$ for the SOM, based on a literature value for the density of SOM produced under similar conditions (i.e., $\alpha$-pinene ozonolysis) and of similar O/C = 0.3.[28]

these mixtures can be altered from those of the pure materials, depending on the physicochemical properties of the components and the particle morphology. For example, dissolution of soluble organic molecules into an aqueous sulfate phase can inhibit crystallization of the inorganic phase.[16−18] Another possibility is that incorporation of an aqueous sulfate solution into an amorphous organic phase can suppress a glass transition of the organic material.[19] In the case that organic and inorganic phase separation occurs within a particle, interactions can be sufficiently limited that the materials effectively behave as they do in their pure states.[20] Thus, the tendency of aqueous inorganic and organic phases to mix is a key property regulating the phase state of the individual constituents in multicomponent particles and ultimately their influence on atmospheric chemical and physical processes.

In the atmosphere, secondary organic material (SOM) makes up a significant fraction of the submicrometer particle mass concentration.[9] SOM production is ultimately tied to the oxidation reactions of volatile organic compounds (VOCs) that produce semi- and low-volatility products. The resulting particle-phase organic material is composed of hundreds to thousands of different molecules. Although SOM is a complex material, a simplifying effort can be made to represent it by a mix of known, individual organic compounds, put together as a model system. The connection between mixing of aqueous ammonium sulfate and organic material and the effect of the organic molecules on the ERH and DRH of ammonium sulfate has been experimentally established for mixtures ranging from approximately 1 to 10 components for a wide range of organic-to-sulfate ratios and molecular structures.[16,17,21,22] The finding is that the phase separation relative humidity (SRH), the ERH, and the DRH of organic and ammonium sulfate mixtures correlate with the oxygen-to-carbon atomic ratio (O/C) of the organic material and the organic-to-sulfate mass ratio (org/sulf) of the mixtures.[16,22] Organic molecules characterized by O/C > 0.7 typically mix (i.e., miscibility) with aqueous ammonium sulfate. The ERH and DRH of ammonium sulfate correspondingly decrease for increasing org/sulf. By comparison, organic molecules of O/C < 0.7 tend to phase separate from aqueous sulfate (i.e., immiscibility), and the DRH and ERH values of ammonium sulfate change little.

Compared to the number of studies using model systems to represent SOM, there are considerably fewer studies on the phase transitions and phase separations in mixed particles of actual SOM and ammonium sulfate. The literature is summarized in Table 1.

Most studies focus on SOM derived from biogenic volatile organic compounds (BVOCs), which account for the production of approximately 90% of global SOM mass concentration, compared to a smaller anthropogenic contribution of 10%.[29] In specific urban regions, however, anthropogenic production can dominate, especially in arid areas. SOM produced from the ozonolysis of terpenes (e.g., $\alpha$-pinene, limonene, and $\beta$-caryophyllene) alters the ERH and DRH by less than 4% RH for organic volume fractions $\varepsilon$ of up to 0.96.[16,20,23] Phase separation of SOM from aqueous ammonium sulfate was inferred from these observations of ERH and DRH and subsequently was confirmed by optical and fluorescence microscopy.[24] By comparison, isoprene photo-oxidation products fully mix with aqueous ammonium sulfate, thereby promoting dissolution of the crystalline ammonium sulfate below the DRH of the pure form and suppressing efflorescence.[18] For this case, the DRH and ERH of ammonium sulfate decrease by over 20% RH for increasing $\varepsilon$.

Production of SOM from the oxidation of aromatic VOCs can dominate the local SOM mass in urban environments or during biomass burning events.[30] Benzene, toluene, and xylene are the most important anthropogenic VOCs with respect to SOM production.[30] Mixed at low volume fractions (i.e., $\varepsilon$ = 0.05–0.16), SOM produced from these precursors does not change the DRH and ERH of ammonium sulfate.[27] For a higher volume fraction of $\varepsilon$ = 0.8, SOM derived from the photo-oxidation of 1,2,4-trimethylbenzene phase separates from aqueous ammonium sulfate.[24] Absent in these prior studies is a systematic account across the full range of organic volume fractions.

In the present study, deliquescence and efflorescence phase transitions and phase separation were investigated for particles composed of ammonium sulfate and SOM produced by toluene photo-oxidation. The particle-phase water content was adjusted by exposure to RHs from <0.5 to 90%. Submicrometer particles having organic volume fractions ranging from 0.0 to 0.9 were


dx.doi.org/10.1021/jp405095e | J. Phys. Chem. A 2013, 117, 8895–8906

studied using hygroscopic tandem differential mobility analysis (HTDMA).[31] Supermicrometer particles were also directly imaged by optical microscopy for low ($\varepsilon$ = 0.12) and high ($\varepsilon$ = 0.8) organic volume fractions to investigate the occurrence of phase separation. The implications of the results with respect to the miscibility or immiscibility of the toluene-derived SOM with aqueous ammonium sulfate are discussed in the context of other types of SOMs, and a collective summary is presented in comparative phase diagrams.

## 2. EXPERIMENTAL SECTION

**2.1. Particle Generation for HTDMA Experiments.** Particles composed of SOM and ammonium sulfate were produced in the Harvard Environmental Chamber (HEC). The HEC, described in King et al.[32] and Shilling et al.,[33] consists of a 4.7 $m^3$ Teflon bag enclosed in a temperature-controlled chamber. The bag was operated as a continuously mixed flow reactor (CMFR), meaning that the inflow and outflow (20 Lpm) were balanced and steady-state conditions were obtained. The mean reactor residence time was 3.9 h, the temperature within the HEC was 25 °C, and the relative humidity $RH^{CMFR}$ in the bag was maintained at either <5 or 40%.

Gaseous toluene, gaseous hydrogen peroxide, and crystalline ammonium sulfate particles were continuously injected into the CMFR. Liquid toluene (DrySolve, purity > 99.8%) was evaporated from the tip of a syringe in a glass round-bottom flask (100 mL, Ace Glass) and carried into the chamber by a pure air flow. Gas-phase concentrations of toluene prior to reaction were 500 ppb ($RH^{CMFR}$ = 40% RH) or 900 ppb ($RH^{CMFR}$ < 5% RH). Hydrogen peroxide solution (Sigma-Aldrich, 30 wt %) was introduced into a separate round-bottom flask by a syringe pump. The hydrogen peroxide evaporated and was flushed into the CMFR by an air flow through the flask to give a gas-phase concentration of ∼10 ppm.

Crystalline ammonium sulfate seed particles (Fluka TraceSELECT, >99.9999% purity) were produced by atomizing (TSI 3076) an aqueous solution of ammonium sulfate and drying the resulting aerosol to less than 30% RH in a silica-packed diffusion drier. The solid polydisperse particles were diameter-classified using a nanodifferential mobility analyzer (nDMA, TSI 3085) and subsequently injected into the CMFR. Particles of +1 charge, having diameters as small as 59 ± 2 nm and as large as 85 ± 2 nm, were classified. The mode diameter was 70 ± 1 nm, and the number concentration was 2.4 (±0.6) × $10^3$ $cm^{-3}$. Doubly charged particles of mode diameter of 101 ± 2 nm also passed through the nDMA and were injected into the CMFR. The range of diameters was 88 ± 3 to 121 ± 4 nm, and the number concentration was 0.9 (±0.3) × $10^3$ $cm^{-3}$.

Radiation from ultraviolet lights on the interior chamber walls induced the photolysis of hydrogen peroxide and hence the production of OH radicals inside of the CMFR. The OH radicals in turn initiated oxidation of toluene. The photo-oxidation chemistry also produced ozone. Low-volatility products from the toluene oxidation condensed as SOM on the surfaces of the ammonium sulfate seed particles, leading to diameter growth. The number-diameter distribution of the mixed ammonium sulfate−organic particles exiting the CMFR was measured throughout an experiment using a Scanning Mobility Particle Sizer (SMPS; TSI 3936).

The particle population exiting the CMFR had a diverse chemical and diameter composition. The residence time of an individual particle within the CMFR was governed by Poisson statistics.[34] For a single input seed diameter, the diameter of a particle exiting the CMFR increased for increased residence time within the chamber. The distribution of particle residence times, coupled with the distribution of seed particle diameters in the CMFR inflow, implied that particles of a single physical diameter in the CMFR outflow corresponded to a distribution of organic volume fractions $\varepsilon$. A particle grown on a singly charged seed particle and having a long residence time within the CMFR could grow to the same diameter as a particle grown on a doubly charged seed particle that had a short residence time in the CMFR. The distribution of $\varepsilon$ at a single diameter was taken into account in the interpretation of the results (cf. section 3.1).

The mass concentration $M_{org}$ and the O/C of the particle-phase organic material were measured using an Aerodyne Aerosol Mass Spectrometer (AMS).[35] For SOM produced at <5% RH, $M_{org}$ was 38 $\mu g\ m^{-3}$, and O/C was 0.72 ± 0.2, taking into account 30% uncertainty in O/C.[35] For SOM produced at 40% RH, $M_{org}$ was 20 $\mu g\ m^{-3}$, and O/C was 0.71 ± 0.2. The fractional contribution of different oxygen−carbon functional groups to the SOM was also modeled using the Master Chemical Mechanism (MCM) (http://mcm.leeds.ac.uk/MCM/download.htt)[36] for each experimental condition.[37]

**2.2. Hygroscopic Tandem Differential Mobility Analyzer (HTDMA).** A HTDMA was used to characterize the properties of the mixed particles of ammonium sulfate and SOM. A quasi-monodisperse particle population was selected by a differential mobility analyzer (DMA) under dry conditions. This subpopulation was subsequently subjected to a RH profile (i.e., initial RH → perturbation RH → final RH). The number-diameter distribution after the RH profile was measured by scanning the voltage of a second DMA while counting the particle number concentration with a condensation particle counter (CPC). The apparatus was as described in ref 18 with the update of the addition of a thermally insulated glass tube. This extension tube, which could be bypassed, allowed variation by an order of magnitude of the time period of RH perturbation from 0.5 to 30 s during a RH profile.

In a typical experiment, an aerosol subflow was sampled from the CMFR outflow, passed through a bipolar diffusion charger (Po-210), and dried to <7% RH in a Nafion conditioner (Perma Pure, PD50T-12SS). The particles in the aerosol flow were classified by a first DMA ($DMA^{mono}$; TSI 3081) maintained at <7% RH and set to pass a mobility equivalent diameter (+1 charge) of $d_{m,+1}^{mono}$. Following $DMA^{mono}$, the RH of the aerosol was adjusted to $RH_1$ in a Nafion conditioner (Perma Pure MD110-96SS; mean residence time $\tau_1$ of 0.5 s). After conditioning to $RH_1$, the aerosol flow either (1) directly entered a second Nafion conditioner ($\tau_2$ = 0.5) that adjusted the aerosol to $RH_2$ or (2) passed first through the extension tube that increased $\tau_1$ to 30 s before entering the second Nafion conditioner. In this way, exposure time $\tau_1$ to $RH_1$ was either 0.5 or 30 s. The raw data underlying the number-diameter distribution $n(d)$ of the particle population in the aerosol flow were then measured using a second differential mobility analyzer $DMA^{filter}$ (TSI 3081) and a CPC (TSI 3010). The sheath flow of $DMA^{filter}$ was maintained at $RH_2$. The CPC recorded the number concentration $N^{filter}$ of particles that was transmitted through $DMA^{filter}$ while the mobility diameter $d_{m,+1}^{filter}$ was scanned. The raw data were analyzed by methods described in the literature to obtain $n(d)$.[18,20,38,39] Taken together, this HTDMA protocol measured $n(d;d_{m,+1}^{mono},RH_1,\tau_1,RH_2)$ of particles exposed to the RH profile of 7% → $RH_1$ → $RH_2$.


dx.doi.org/10.1021/jp405095e | J. Phys. Chem. A 2013, 117, 8895−8906

**Table 2. Experimental Conditions of This Study**[a]

| experiment | type | $RH^{CMFR}$ (%) | $d^{mono}_{m,+1}$ (nm) | $RH_1$ (%) | $\tau_1$ (s) | $RH_2$ (%) |
|---|---|---|---|---|---|---|
| 1 | R | 40 | 75*, 90*, 190* | 50−85 | 0.5 | 50−85 |
| 2 | R | 40 | 75*, 90*, 190* | 50−85 | 30 | 50−85 |
| 3 | D | 40 | 90, 190 | 50−85 | 0.5 | 50−85 |
| 4 | D | 40 | 90, 190 | 50−85 | 30 | 50−85 |
| 5 | E | 40 | 75*, 90*, 190* | 10−50 | 0.5 | 50 |
| 6 | E | 40 | 75*, 90*, 190* | 10−50 | 30 | 50 |
| 7 | R | <5 | 75*, 90*, 190* | 50 | 0.5 | 50 |
| 8 | R | <5 | 75*, 90*, 190* | 50 | 30 | 50 |
| 9 | D | <5 | 90, 190 | 50−85 | 0.5 | 50−85 |
| 10 | D | <5 | 90, 190 | 50−85 | 30 | 50−85 |
| 11 | E | <5 | 75*, 90*, 190* | 10−50 | 0.5 | 50 |
| 12 | E | <5 | 75*, 90*, 190* | 10−50 | 30 | 50 |

[a]An asterisk (*) indicates that the particle population was deliquesced following size selection by $DMA^{mono}$. Experiment types R, D, and E denote measurements of reference number-diameter distributions (eq 1), tests for deliquescence (eq 2), and tests for efflorescence (eq 3), respectively.

For a single measurement of $n(d)$, the values of $d^{mono}_{m,+1}$, $RH_1$, $\tau_1$, and $RH_2$ were kept constant. Across a set of experiments, one or more of these values was co-varied (cf. Table 2). For example, in experiment #3 of Table 2, $RH_1$ and $RH_2$ were initially set to 50% RH, and $n(d)$ was recorded as $d^{mono}_{m,+1}$ was switched stepwise from 75, to 90, to 190 nm in a set of three measurements. $RH_1$ and $RH_2$ were subsequently incremented by 5% RH to 55% RH, and $n(d)$ was again recorded for the three values of $d^{mono}_{m,+1}$. This set of measurements, constituting experiment #3, was continued until $RH_1$ and $RH_2$ were 85% RH. Further details of each set of experiments are described in sections 2.2.1 ("R"), 2.2.2 ("D"), and 2.2.3 ("E"). The labels R, D, and E represent the type of experiments noted in Table 2 and correspond to measurements of reference number-diameter distributions, tests for deliquescence, and tests for efflorescence, respectively. A layout of the experiments, showing the RH of each component for the three types of experiments R, D, and E, is shown in Figure 1.

*2.2.1. Reference Distribution.* Reference distributions (Figure 1, row 1) were obtained by measuring the number-diameter distribution of fully aqueous particle populations from 50 to 85% RH. Following classification by $DMA^{mono}$, a particle population was deliquesced at 90% RH. The particles were subsequently exposed to RHs between 50 and 85%. The Nafion conditioners were maintained at the same RH (i.e., $RH_1 = RH_2$). The RH protocol was as follows:

$$RH^{CMFR} \rightarrow 7\% \rightarrow d^{mono}_{m,+1} \rightarrow 90\% \rightarrow (RH_1\text{: } 50\text{−}85\%) \rightarrow (RH_2\text{: } 50\text{−}85\%) \rightarrow n(d;\ RH_2) \quad (1)$$

Particles of pure aqueous ammonium sulfate do not effloresce for RH > 35%.[7] For the mixed particles studied by eq 1 in the range of RH from 50 to 85%, the ammonium sulfate component of the reference measurement was therefore assumed to be fully aqueous (i.e., no particles effloresced for RH ≥ 50%). The data set of the efflorescence test (cf. sections 2.2.3 and 3.2 and Figure 3) validated this assumption.

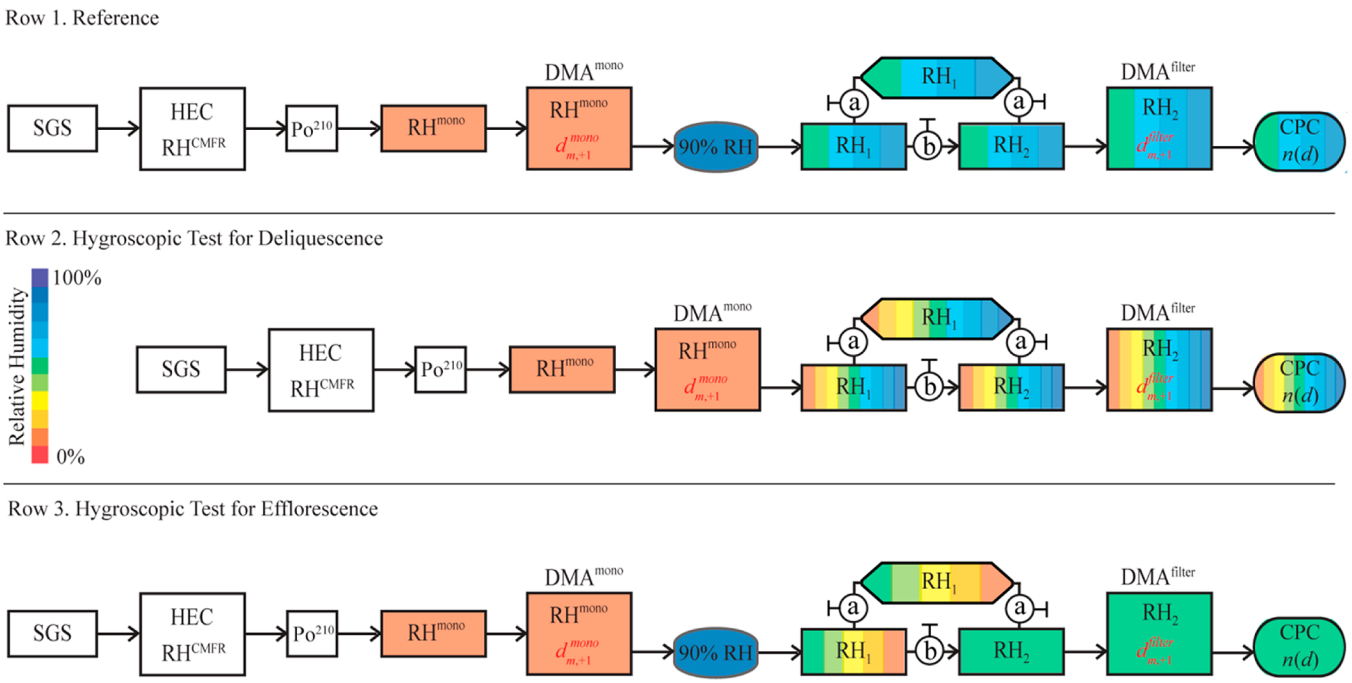


**Figure 1.** Schematic diagram of the HTDMA experimental setup. Labeled components include the sulfate seed particle generation system (SGS), the HEC, a polonium-210 charger ($Po^{210}$), RH adjustment in Nafion tubes, DMAs, and CPC. Components of the HTDMA are colored to represent the local RH (see color bar) during each type of experiment R, D, and E (rows 1−3; cf. Table 2 and section 2.2). Rainbow shading within a single component indicates that the RH was scanned during the measurements. Circles labeled a and b represent control of the aerosol flow path through the HTDMA. When valve a was closed and valve b was open, the exposure time of the aerosol to $RH_1$ was 0.5 s. When valve a was open and valve b was closed, the exposure time of the aerosol to $RH_1$ was 30 s.


dx.doi.org/10.1021/jp405095e | J. Phys. Chem. A 2013, 117, 8895−8906

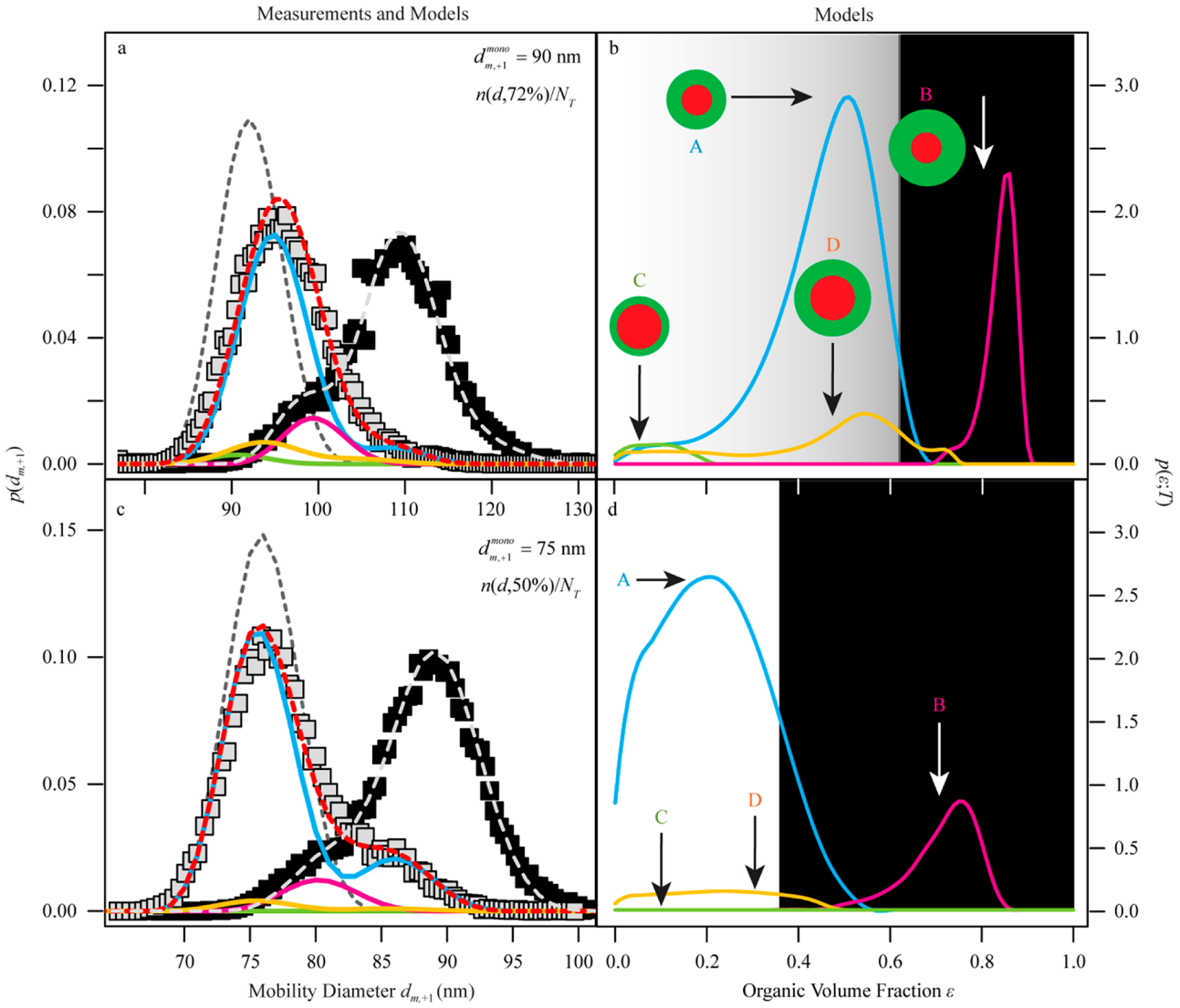


**Figure 2.** (a) Measured and modeled probability density functions $p(d_{m,+1})$ of number-diameter distributions of particle populations that underwent tests for efflorescence and deliquescence. Black squares show a particle population for which the ammonium sulfate within all particles is fully deliquesced (i.e., the reference distribution at 72% RH). Gray squares represent a particle population that underwent a test for deliquescence at 72% RH (cf. eq 2). The population was composed of particles containing fully deliquesced ammonium sulfate for $\varepsilon \geq \varepsilon_D(72\%)$ and particles containing crystalline ammonium sulfate for $\varepsilon < \varepsilon_D(72\%)$. Solid lines represent the result of the hygroscopic model for each particle type $T$ represented in panel b. Dashed lines show the model results for the sum across the entire population; the red dashed line, which is the sum of the four colored solid lines, represents the best-fit of the hygroscopic model to the measurement. The short-dashed and long-dashed gray lines show model results for particle populations in which the ammonium sulfate components are crystalline or aqueous, respectively. (b) The probability density functions $p(\varepsilon;T)$ of organic volume fractions for particle types $T$ for the particle subpopulations that make up the full particle population classified by $DMA^{mono}$. The colorized circles A through D represent pictorally the four particle types treated in the hygroscopic model. SOM is shown in green, and ammonium sulfate is shown in red. Shading from white to black in the background of the panel indicates the dissolved fraction of ammonium sulfate for increasing $\varepsilon$, ranging from zero at $\varepsilon = 0$ (white) to unity at $\varepsilon \geq \varepsilon_D$ (black). (c,d) Panels c and d are as described for panels a and b, with the change that gray squares represent a particle population exposed to a test for efflorescence at 26% RH. The RH profile was 7% → 90% → ($RH_1$: 26%) → ($RH_2$: 50%). The red dashed line of panel c represents the hygroscopic model optimized for $\varepsilon_E(26\%)$.

*2.2.2. Test for Deliquescence.* Deliquescence phase transitions from 50 to 85% RH were probed by measuring $n(d;RH_2)$ of a particle population for 50% < $RH_2$ < 85% (Figure 1, row 2). The RH protocol employed to test for deliquescence (eq 2) was as described for the reference distribution, with the exception that particles were not deliquesced following classification by $DMA^{mono}$.

$$RH^{CMFR} \rightarrow 7\% \rightarrow d^{mono}_{m,+1} \rightarrow (RH_1\text{: } 50\text{–}85\%) \rightarrow (RH_2\text{: } 50\text{–}85\%) \rightarrow n(d;\ RH_2) \quad (2)$$

In the case that at least some of the particles in the population did not deliquesce, the distribution $n(d)$ measured for a deliquescence test at $RH_2$ would shift to smaller diameters compared to the reference distribution at $RH_2$. The data analysis also took into consideration that some particles did not effloresce even to 7% RH (cf. section 3.1).

*2.2.3. Test for Efflorescence.* Following classification by $DMA^{mono}$, particles were deliquesced at 90% RH and subsequently exposed to values of $RH_1$ between 50 and 10% RH (Figure 1, row 3). After conditioning to $RH_1$, the particle population was equilibrated to $RH_2$ = 50%, and $n(d;50\%)$ was


dx.doi.org/10.1021/jp405095e | J. Phys. Chem. A 2013, 117, 8895–8906

measured. The RH protocol used to test for efflorescence is given by eq 3.

$$\mathrm{RH}^{\mathrm{CMFR}} \rightarrow 7\% \rightarrow d_{\mathrm{m},+1}^{\mathrm{mono}} \rightarrow 90\% \rightarrow (\mathrm{RH}_1\text{: } 50-10\%) \rightarrow (\mathrm{RH}_2\text{: } 50\%) \rightarrow n(d;\ 50\%) \quad (3)$$

For an efflorescence test, in the case that at least some particles effloresced at $\mathrm{RH}_1$, $n(d;50\%)$ would shift to smaller diameters relative to the reference distribution at 50% RH. The particle population was conditioned to 50% RH following the test for efflorescence at $\mathrm{RH}_1$ to increase the diameter separation between crystallized and aqueous particles (i.e., due to hygroscopic growth), thereby improving detection of efflorescence transitions. This approach was valid provided that deliquescence of mixed particles did not occur as low as 50% RH, including to high organic volume fractions, as supported by the observations (cf. section 3.1).

**2.3. Optical Microscopy Experiments.** The apparatus and procedures of the optical microscopy experiments were described previously in ref 24. Briefly, SOM was produced in the HEC for $\mathrm{RH}^{\mathrm{CMFR}} < 5\%$ (cf. section 2.1) but in the absence of seed particles and at a higher organic mass concentration $M_{\mathrm{org}}$ of either 45 or 100 $\mu$g m$^{-3}$. Approximately 1 mg of SOM was collected on quartz filters (Whatman 1851-047) (8 L pm flow, 48 h collection time, sealed filter casing). The SOM was extracted from the filters in high-purity water (18.2 MΩ cm; 30 mL). Ammonium sulfate was added to the extract to prepare organic-to-sulfate mass ratios of 0.11 ($M_{\mathrm{org}}$ = 45 $\mu$g m$^{-3}$) or 3.0 ($M_{\mathrm{org}}$ = 100 $\mu$g m$^{-3}$), corresponding to respective organic volume fractions of 0.12 and 0.80 for an SOM density of 1400 kg m$^{-3}$.[40] Solutions of pure ammonium sulfate and pure SOM were also prepared as reference points in the analysis. The prepared solutions were atomized onto Teflon slides, resulting in particles having diameters from 28 to 40 $\mu$m. The slide was placed in a temperature- and RH-controlled cell. Optical images were recorded at 289.5 K while scanning the RH from 90 to 30% at a rate of 0.5−2.0% min$^{-1}$. In cases that efflorescence occurred, RH was subsequently increased and scanned from 60 to 85% RH at a rate of 0.5−0.6% min$^{-1}$ to observe deliquescence. In cases that efflorescence was not observed at RH ≥ 30%, RH was further decreased at a faster rate of 4−5% RH min$^{-1}$ to less than 0.5%.

Because the SOM was extracted from the filters in water, only the water-soluble fraction of the SOM was studied in the microscopy experiments.[24] This material may be enriched in more-oxidized organic species compared to the total SOM collected on the filter. More-oxidized species compared to less-oxidized species tend to favor mixing with an aqueous phase. An implication is that phase separation for the water-soluble fraction suggests phase separation for the whole fraction.[24]

## 3. RESULTS AND DISCUSSION

**3.1. Hygroscopic Modeling of Number-Diameter Distributions.** The number-diameter distribution of the ammonium sulfate seed particles, taken together with the distribution of individual particle residence times within the CMFR, implies a distribution of organic volume fraction $p(\varepsilon)$ at each particle diameter exiting the CMFR. Therefore, to interpret hygroscopic behavior that depends on $\varepsilon$, $p(\varepsilon)$ must be determined for the investigated particle diameters. The two most abundant particle subpopulations in the CMFR outflow are those grown on +1 and +2 seed particles. These particles when exiting the CMFR are then recharged to an equilibrium charge distribution prior to entering the HTDMA. Particles carrying +1 and +2 charges are transmitted by $\mathrm{DMA}^{\mathrm{mono}}$. As a result, there are four principal subpopulations of particle types $T$ exiting $\mathrm{DMA}^{\mathrm{mono}}$ including A: +1/+1, B: +1/+2, C: +2/+1, and D: +2/+2, denoting type, the initial charge/the recharge. In further detail, for typical experimental conditions, the particle types listed in order of decreasing fractional contribution to the population are as follows: A, singly charged mixed SOM/sulfate particles grown on sulfate seeds of mode diameter 70 ± 1 nm; B, doubly charged mixed particles having seeds of mode diameter 70 ± 1 nm; C, singly charged mixed particles having seeds of mode diameter 101 ± 2 nm; and D, doubly charged mixed particles having seeds of mode diameter 101 ± 2 nm.

On the basis of measurements of the number-diameter distribution of the seed particles and of the particle population exiting the CMFR, the probability density function $p(\varepsilon;T)$ of organic volume fraction $\varepsilon$ for each particle type $T$ is obtained by inversion modeling.[18,20] Examples of the four modeled $p(\varepsilon;T)$ are shown in Figure 2 for $d_{\mathrm{m},+1}^{\mathrm{mono}}$ = 90 nm (panel b). In the case that the transmission window of $\mathrm{DMA}^{\mathrm{mono}}$ for singly charged particles does not overlap any diameters of doubly charged seed particles, particle type C is absent. (As an example of the latter case, for $d_{\mathrm{m},+1}^{\mathrm{mono}}$ = 75 nm in panel d of Figure 2, singly charged particles of diameters from 71 to 80 nm are transmitted by $\mathrm{DMA}^{\mathrm{mono}}$. Particles of type C, though singly charged, have diameters of 88 nm and larger. Particle type C is therefore absent in $p(\varepsilon;T)$ for $d_{\mathrm{m},+1}^{\mathrm{mono}}$ = 75 nm.)

The distribution of organic volume fractions in the quasi-monodisperse particle population transmitted by $\mathrm{DMA}^{\mathrm{mono}}$ implies that a range of $\varepsilon$ values is probed for a single measurement of $n(d;\mathrm{RH})$. Definitions $\varepsilon_{\mathrm{D}}(\mathrm{RH})$ and $\varepsilon_{\mathrm{E}}(\mathrm{RH})$ are introduced for a population; particles of $\varepsilon \geq \varepsilon_{\mathrm{D}}(\mathrm{RH})$ are deliquesced, and particles of $\varepsilon \leq \varepsilon_{\mathrm{E}}(\mathrm{RH})$ are effloresced. Particles of $\varepsilon_{\mathrm{E}}(\mathrm{RH}) < \varepsilon < \varepsilon_{\mathrm{D}}(\mathrm{RH})$ can be either effloresced or deliquesced depending on the RH profile of the experiment. They are effloresced in the case of a deliquescence test (eq 2) and deliquesced in the case of an efflorescence test (eq 3).

These multiple complexities in the particle population imply that a hygroscopic model that accounts for $p(\varepsilon;T)$ at each diameter is needed to extract curves of $\mathrm{ERH}(\varepsilon)$ and $\mathrm{DRH}(\varepsilon)$ from measurements of $n(d;\mathrm{RH})$. As described in Smith et al.,[18] the number-diameter distribution $n(d;\mathrm{RH})$ of the particle population is modeled by taking into account the number-diameter-composition distribution $n(d,\varepsilon;T)$ of particles transmitted through $\mathrm{DMA}^{\mathrm{mono}}$ and their subsequent hygroscopic processing by deliquescence or efflorescence tests (eqs 2 and 3). The model-measurement difference $\Delta n(d;\mathrm{RH})$ is minimized by optimizing the values of $\varepsilon_{\mathrm{D}}(\mathrm{RH})$ and $\varepsilon_{\mathrm{E}}(\mathrm{RH})$ in the model.

The diameter-based hygroscopic growth factor $g$ of a particle in the model is calculated based on the undissolved portion of crystalline ammonium sulfate (i.e., growth factor of 1), the growth factor $g_0$ of dissolved aqueous ammonium sulfate, and the growth factor $g_1$ of toluene-derived SOM, as follows:[18]

$$g(y;\ \varepsilon) = [(1-\varepsilon)(1 + (g_0^3(y) - 1)f) + \varepsilon g_1^3(y)]^{1/3} \quad (4)$$

for $y$ = RH/100. The term $f$ is the fraction of ammonium sulfate that is dissolved. For aqueous ammonium sulfate, $g_0$ of ref 41 is used. The SOM growth factor $g_1(\mathrm{RH})$ is obtained by inversion against the measurements of the hygroscopic growth of fully aqueous particle populations of $d_{\mathrm{m},+1}^{\mathrm{mono}}$ = 190 nm (section 2.2.1). For this large diameter, the volume contribution by ammonium


dx.doi.org/10.1021/jp405095e | J. Phys. Chem. A 2013, 117, 8895−8906

sulfate is <6%, implying that the observed hygroscopic response is attributable almost entirely to SOM, although the small contribution by ammonium sulfate is also included in the inversion analysis as $g_0$ (Figure S1, Supporting Information). After inversion, the parametrization for $g_1$ of toluene-derived SOM is as follows: $g_1(y) = 1 + A(1 - y)^{-B}y^C$ for $A = 0.0697$, $B = 0.740$, and $C = 1.976$. Water uptake by aqueous ammonium sulfate and SOM is treated independently, implying that the thermodynamic excess volume of mixing is approximated as zero.[42] In this case, water uptake is modeled as the same for both phase-separated and phase-mixed particles. The acceptability of this assumption is supported by agreement of the results of the hygroscopic model with the measurements for a range of $p(\varepsilon)$ and RH (Figure S2).

For the reference distribution, all particles are completely aqueous, and $f = 1$. For a deliquescence test, the dissolved fraction of a particle bin in the model is regulated by the liquidus curve DRH($\varepsilon$), as follows:[18,42]

$$f(y;\ \varepsilon) = \begin{cases} \dfrac{\varepsilon(1 - \varepsilon_D)}{\varepsilon_D(1 - \varepsilon)} & \text{for } \varepsilon < \varepsilon_D(y) \\ 1 & \text{for } \varepsilon \geq \varepsilon_D(y) \end{cases} \quad (5)$$

For an efflorescence test, the dissolved fraction of a particle bin in the model is regulated by the efflorescence curve ERH($\varepsilon$), as follows:

$$f(y;\ \varepsilon) = \begin{cases} 0 & \text{for } \varepsilon \leq \varepsilon_E(y) \\ 1 & \text{for } \varepsilon > \varepsilon_E(y) \end{cases} \quad (6)$$

Although eq 5 strictly holds for effloresced particles too, the simplification $f = 0$ is used because $\varepsilon_D(y) \rightarrow 1$ for $y < 0.35$ (Figure 3).

The model of hygroscopic growth reproduces well the measured reference distributions as well as the $n(d;\text{RH})$ measurements of the efflorescence tests for RHs of 50−85% over the full range of $\varepsilon$ (Figures S1 and S2). The hygroscopic model overestimates diameters for $\varepsilon < \varepsilon_D$ compared to measurements (i.e., modeled $n(d;\text{RH})$ is right-shifted) for some of the number-diameter distributions of deliquescence tests (Figure S3). A possible explanation for the overestimate is that the sulfate components in some particles, especially those of high organic volume fraction, are kinetically isolated from gas-phase water and therefore do not grow hygroscopically. In this case, instead of following eqs 4 and 5, $f = 0$ for these particles, meaning that only the organic material contributes to growth factor $g$ in eq 4.

The fraction $z(\varepsilon)$ of particles having sulfate components that are inaccessible to gas-phase water is defined in the model as an increasing function of $\varepsilon$ as follows

$$z(\varepsilon) = \begin{cases} 0 & \text{for } \varepsilon < -\dfrac{b}{m} \\ m\varepsilon + b & \text{for } -\dfrac{b}{m} \leq \varepsilon \leq -\dfrac{(1 - b)}{m} \\ 1 & \text{for } \varepsilon > -\dfrac{(1 - b)}{m} \end{cases} \quad (7)$$

where $m$ and $b$ are constants for one experimental condition. Their values are obtained by minimization of the model-measurement difference $\Delta n(d;\text{RH})$ (cf. Figures S4 and S5 and

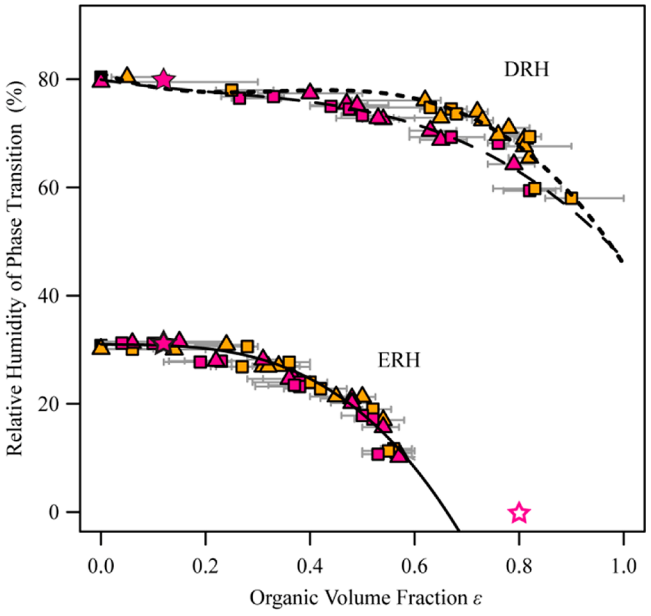


**Figure 3.** Deliquescence and efflorescence RHs of particles composed of ammonium sulfate and SOM produced from toluene photooxidation. Data derived from HTDMA measurements are shown for $\text{RH}^{\text{CMFR}}$ = 40% (orange) and $\text{RH}^{\text{CMFR}}$ < 5% (magenta). Squares correspond to data of $\tau_1 = 0.5$ s and triangles to data of $\tau_1 = 30$ s. Error bars represent uncertainty in the RH and particle sizing (see the main text). Also shown are data derived from experiments based on optical microscopy (stars). The ERH results from the microscopy data are offset plotted to 4% RH lower than measured to compensate for the difference between the HTDMA (ERH = 31%) and microscopy techniques (ERH = 35%) for the observed ERH of pure ammonium sulfate. The open star indicates an experiment that was conducted but for which no efflorescence was observed, even at a RH of ≤0.5%.

associated discussion). An implication of eq 7 is that there are a variety of morphologies in the particle population so that for a fixed organic volume fraction, some particles have sufficiently accessible ammonium sulfate for deliquescence to take place ($f$ given by eq 5) whereas other particles do not ($f = 0$).

**3.2. Phase of Mixed Particles.** Figure 2a shows the measured (gray squares) number-diameter distributions for a test of deliquescence at 72% RH. Data are shown for $d_{m,+1}^{\text{mono}} = 90$ nm for the conditions of experiment #4 (cf. Table 2). Also plotted are data representing a fully deliquesced particle population at 72% RH (black squares; reference distribution; $g_0 = 1.37$ and $g_1 = 1.09$ at 72% RH). The gray points are shifted to smaller diameters compared to the black points, indicating that some particles within the population have crystalline ammonium sulfate components (i.e., $g_0 = 1$ and $g_1 = 1.09$ for $\varepsilon < \varepsilon_D(72\%)$ and $g_0 = 1.37$ and $g_1 = 1.09$ for $\varepsilon \geq \varepsilon_D(72\%)$).

Gray dashed lines of Figure 2a represent the results of the hygroscopic models for particle populations having fully crystalline (short-dashed gray) or fully aqueous (long-dashed gray) ammonium sulfate components. The figure shows that the case of fully aqueous ammonium sulfate (i.e., the reference distribution) is well predicted by the hygroscopic model. The model case of fully crystalline ammonium sulfate, however, does not match data recorded at 72% RH. Instead, for the data set of the deliquescence test, a model line (red dashed) is shown that optimizes the value of $\varepsilon_D(72\%)$ to maximize the model-measurement agreement, meaning that particles of $\varepsilon < \varepsilon_D(72\%)$ have at least some crystalline ammonium sulfate and


dx.doi.org/10.1021/jp405095e | J. Phys. Chem. A 2013, 117, 8895−8906

that particles of $\varepsilon \geq \varepsilon_D(72\%)$ have fully aqueous ammonium sulfate. Plotted in Figure 2b is $p(\varepsilon;T)$ of each particle type. This model provides good agreement with the recorded data of the deliquescence test for an optimized value of $\varepsilon_D(72\%) = 0.73$. Solid lines of Figure 2a show separately the modeled number-diameter distributions for particle types A−D. Thus, the interpretation of the data of Figure 2a is that particles of $\varepsilon \geq 0.73$ are deliquesced at 72% RH. This result appears as the point $\mathrm{DRH}(0.73^{+0.04}_{-0.02}) = 72\%$ in Figure 3. The uncertainty analysis of DRH follows that described in Smith et al.[18] The uncertainty estimates take into account measurement uncertainties of ±1% RH as well as of ±1 nm in $n(d)$ for each of the seed particle population, the quasi-monodisperse particle population selected by $\mathrm{DMA}^{\mathrm{mono}}$, and the particle population measured by $\mathrm{DMA}^{\mathrm{filter}}$.

An example of a test for efflorescence at 26% RH is shown in Figure 2c for $d^{\mathrm{mono}}_{\mathrm{m},+1} = 75$ nm (experiment #12 in Table 2). The gray squares show a number-diameter distribution of a particle population deliquesced at 90% RH, dried to 26% RH and conditioned to 50% RH (eq 3). Black squares represent the reference distribution at 50% RH (i.e., fully aqueous components of ammonium sulfate). The leftward shift of the gray squares compared to the black squares indicates that some particles within the population of the efflorescence test have crystalline ammonium sulfate components. Plotted in Figure 2d are $p(\varepsilon;T)$ of each particle type that contributes to the particle population. The value of $\varepsilon_E(26\%)$ that optimizes the fit of the model (red dashed line) to the gray data points is 0.36, meaning that particles of $\varepsilon \leq 0.36$ effloresce at 26% RH. This result appears as the point $\mathrm{ERH}(0.36^{+0.04}_{-0.05}) = 26\%$ in Figure 3.

The DRH($\varepsilon$) and ERH($\varepsilon$) values for all experiments are summarized in Figure 3. Table S1 lists the data points. Table S2 provides power-law parametrizations of the data sets. The trend is that, compared to the pure ammonium sulfate values of DRH = 79.5% and ERH = 30−35%, the deliquescence and efflorescence phase transitions of the mixed particles decrease as the organic volume fraction increases. The data for low $\varepsilon$ are consistent with the report of Kleindienst et al.[27] for $\varepsilon = 0.16$ of a negligible influence of toluene photo-oxidation SOM on the DRH and ERH of ammonium sulfate. The data points of Figure 3 are delineated by $\tau_1 = 0.5$ (squares) and 30 s (triangles). They show no influence of humidification (i.e., for DRH) or drying (i.e., for ERH) times on the phase transitions, at least for the 60-fold range probed for $\tau_1$ from 0.5 to 30 s. Orange and magenta symbols represent the data for $\mathrm{RH}^{\mathrm{CMFR}}$ of 40 and <5%, respectively. Within measurement uncertainty, the efflorescence data do not depend on the RH of SOM production (i.e., $\mathrm{RH}^{\mathrm{CMFR}}$; cf. Figure S6. Therefore, a single parametrization of ERH($\varepsilon$) is reported in Table S2. The hygroscopic growth factors $g_1$ for the SOM produced at the two $\mathrm{RH}^{\mathrm{CMFR}}$ values, as well as at the two $\tau$ values, also do not differ from one another.

Even so, for $\varepsilon > 0.5$, the DRH values for particles produced at <5% RH are measurably offset by −3 to −5% RH compared to the values for particles produced at 40% RH (cf. Figure S7. These results could suggest that there are chemical differences between the two types of SOMs. Neither the measured O/C values (0.72 ± 0.2 and 0.71 ± 0.2, respectively) nor the fractional contributions of different organic functional groups to the SOM modeled by the MCM (Figure S8), however, differentiate the SOMs produced at the two RH values. One possibility is that there are nevertheless chemical differences sufficient to alter DRH but insufficient for detection at the coarse resolution of an O/C ratio or within the chemistry included in the MCM.

A comparison of the results of this study to other measurements reported in the literature of ERH and DRH of ammonium sulfate mixed with different types of SOM is shown in Figure 4. Deliquescence and efflorescence of ammonium

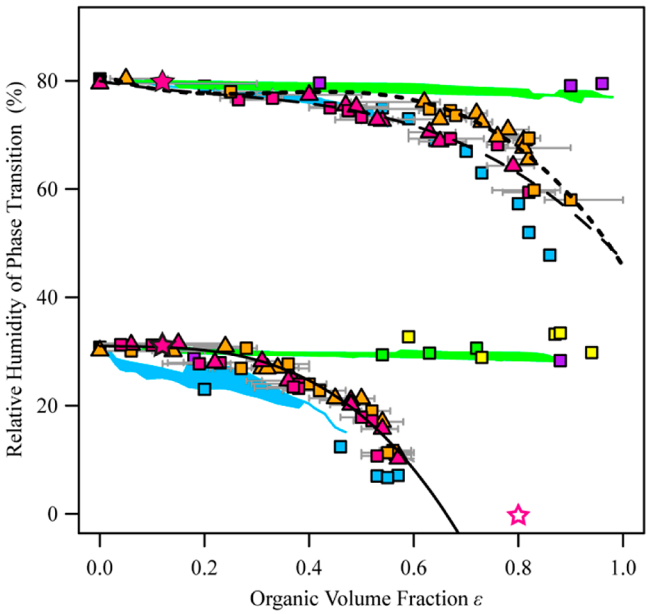


**Figure 4.** Comparison of DRH and ERH results of this study to those reported in the literature for other types of SOM mixed with ammonium sulfate. Orange and magenta points show results for toluene photo-oxidation products (this study; Figure 3). Literature results are shown for SOM produced by α-pinene ozonolysis (green shading;[20] green points[23]), limonene ozonolysis (yellow points[23]), β-caryophyllene ozonolysis (purple points[16]), and isoprene photo-oxidation (blue points and shading[18]).

sulfate mixed with toluene-derived SOM occur at RH values equal to or lower than those of ammonium sulfate mixed with products of terpene ozonolysis and at RH values equal to or higher than those of ammonium sulfate mixed with products of isoprene photo-oxidation. Differences in oxygen-to-carbon ratios and specific oxygen−carbon functional groups among the different SOMs might explain the differing phase transition behaviors. Higher O/C values can be associated with more hygroscopic SOM, implying greater favorability for mixing with an aqueous sulfate phase and, consequently, greater influence of the SOM on the deliquescence and efflorescence phase transitions of ammonium sulfate. For the data of Figure 4, the O/C value of toluene-derived and isoprene-derived SOM is 0.7 ± 0.2, whereas that of α-pinene-derived SOM is 0.4 ± 0.1.

Optical microscopy images were collected to probe visually for phase separation, deliquescence, and efflorescence transitions at low ($\varepsilon = 0.12$) and high ($\varepsilon = 0.8$) organic volume fractions (Figure 5). For comparison to the images presented for ammonium sulfate mixed with toluene-derived SOM, examples are shown of particles consisting of a single homogeneous phase [pure ammonium sulfate, Figure 5 and Movie S1, and pure toluene photo-oxidation SOM, Figure S9] and a two-phase coating-core morphology (ammonium sulfate mixed with α-pinene ozonolysis SOM, Figure S9, adapted from You et al.[24]).


dx.doi.org/10.1021/jp405095e | J. Phys. Chem. A 2013, 117, 8895−8906

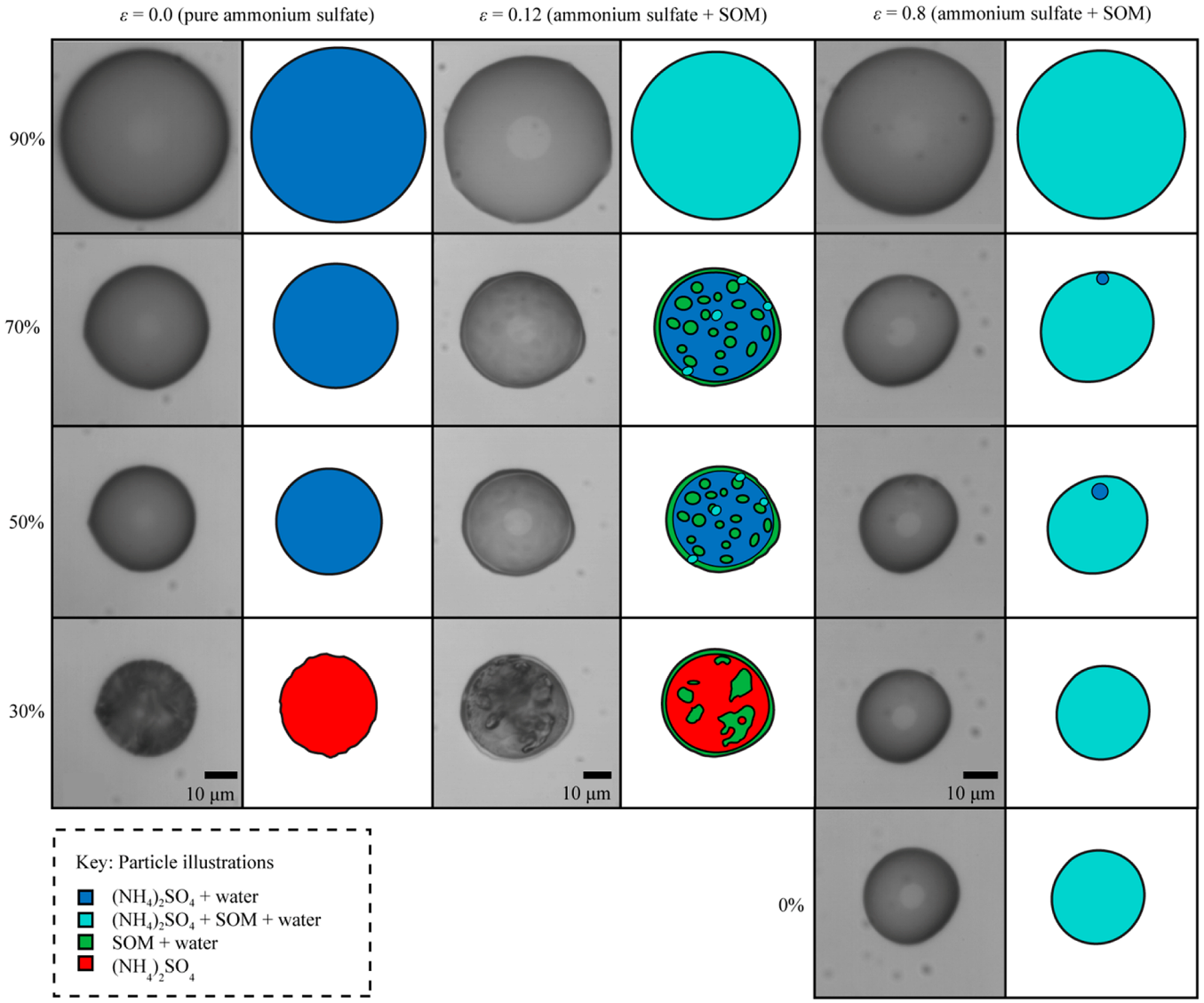


**Figure 5.** Optical microscopy images for decreasing RH (also cf. Movies S1−S3). Columns from left to right represent increasing organic volume fractions $\varepsilon$ of toluene-derived SOM mixed with ammonium sulfate. Images are shown in columns 1, 3, and 5. Illustrations of the images are shown in columns 2, 4, and 6 for clarity. The diameters of the deposited particles at 30% RH range from 28 to 40 $\mu$m (cf. scale bars in row 4).

The optical images recorded for particles of $\varepsilon$ = 0.12 (Figure 5, column 3 and Movie S2) for decreasing RH show that one phase separates into two phases by 85 ± 5% RH. For this composition, the second phase forms both as an outer layer and as inclusions. The inclusions could either be within the particle volume (i.e., akin to an emulsion) or located at the particle−air interface. Similar phase-separated morphologies have been observed in experiments probing liquid−liquid phase separation for particles containing ammonium sulfate mixed with one or a few organic species.[21,43] A possible mechanism for the formation of the phase-separated inclusions is spinodal decomposition.[43] The phase-separated morphologies of the submicrometer aerosol particles studied by HTDMA could be different from those of supermicrometer supported particles studied in the microscopy experiments (e.g., the number of inclusions is expected to decrease with decreasing particle diameter).[21,44] The RH of phase separation, however, is not expected to change with particle diameter.[20,24,45,46]

When the RH is decreased to 35.4 ± 0.6%, the ammonium sulfate in the particle effloresces. This observation is consistent with the ERH values derived from HTDMA experiments, taking into account the 4% offset in the observed ERH of pure ammonium sulfate for the HTDMA (ERH = 31%) and microscopy (ERH = 35%) techniques. This difference is believed to be explained by the larger particle sizes and longer observation times used for the microscopy experiments.[7,16] The ERH values measured by optical microscope techniques (i.e., particles supported on a substrate) agree well with those measured for suspended particles when similar particle diameters and observation times are compared,[47,48] which implies that the substrate does not influence the RH of efflorescence. For increasing RH, the ammonium sulfate components deliquesce at RH = 80 ± 2%, also consistent with the HTDMA measurements.

For particles of $\varepsilon$ = 0.8, the images (cf. Movie S3) show that for decreasing RH, one phase may separate into one major phase and one minor phase at a RH between 100 and 70%. In this case, the second phase appears as a small particle within or on the larger droplet. By mass balance, most of the organic and inorganic material is in the major mixed phase. The minor


dx.doi.org/10.1021/jp405095e | J. Phys. Chem. A 2013, 117, 8895−8906

phase may result from saturation of the mixed phase. Estimates based on five movies of particles of $\varepsilon = 0.8$ suggest that the minor phase is absent below roughly 50−20%, indicating that reduced water content favors mixing. Consistent with the mixing, efflorescence of ammonium sulfate is not observed in the particles as the RH is decreased to below 0.5%.

## 4. CONCLUSIONS

The results of this study are summarized as follows. (1) SOM produced by toluene photo-oxidation decreases the ERH and DRH of ammonium sulfate in mixed particles as the organic volume fraction increases from 0.0 to 0.9 (Figure 3). (2) The deliquescence and efflorescence phase transitions of the mixed particles are not changed by RH exposure time, at least over the time scales investigated of 0.5−30 s. (3) For $\varepsilon > 0.5$, the DRH values for particles produced at <5% RH were measurably offset by −3 to −5% RH compared to the values for particles produced at 40% RH, implying a dependence of SOM water uptake properties on the production RH (Figure 3 and Figure S7). (4) Aqueous ammonium sulfate and toluene-derived SOM phase separate for a low organic volume fraction (Figure 5).

The behaviors for different types of SOMs can be compared. The results of this study show that aqueous ammonium sulfate and toluene photo-oxidation SOM can either partially separate or mix, depending on the RH and organic volume fraction. Optical images of Figure 5 show phase separation into an ammonium-sulfate-rich phase and an organic-rich phase at RH < 85% for $\varepsilon = 0.12$. Consequently, there is a negligible effect of the SOM on the phase transitions of ammonium sulfate for particles of low $\varepsilon$. The decrease in ERH below that of pure ammonium sulfate indicates that significant mixing of aqueous ammonium sulfate and SOM occurs at RH $\leq$ 30% for $\varepsilon > 0.2$. For comparison, aqueous ammonium sulfate and $\alpha$-pinene ozonolysis SOM separate into nearly pure inorganic and organic phases for RH $\geq$ 90% for a wide range of organic volume fractions. As a consequence, there is a weak effect of SOM on the ERH of ammonium sulfate.[20,23] For further comparison, aqueous ammonium sulfate and isoprene photo-oxidation SOM mix for RH $\geq$ ERH($\varepsilon$).[18]

Phase diagrams summarizing the foregoing and highlighting the miscibility regions for aqueous ammonium sulfate mixed with these three different types of SOM are represented in Figure 6. Diagrams are constructed based on data of Figure 4, images of Figure 5, and results from You et al.[24] Large regions of the diagrams are metastable with respect to crystalline ammonium sulfate (i.e., RH < DRH($\varepsilon$)). Figure 6 demonstrates that the phase diagram of particles of ammonium sulfate and toluene-derived SOM is intermediate to those of ammonium sulfate mixed with either $\alpha$-pinene ozonolysis SOM (i.e., phase separation) or isoprene photo-oxidation SOM (i.e., phase mixing).

These results also update to a certain degree the predictions for phase separation based on O/C as given in Bertram et al.[16] and Song et al.[22] In these references, SRH was parametrized as independent of the organic volume fraction. In the case of $\alpha$-pinene-derived and isoprene-derived SOM, this simplification proves acceptable. The SRH predicted by both parametrizations for aqueous ammonium sulfate and $\alpha$-pinene-derived SOM is 96% RH,[16,22] consistent with the representation in Figure 6. For aqueous ammonium sulfate and isoprene photo-oxidation SOM, the parametrization by Bertram et al.[16] predicted a SRH between approximately 50 and 0% RH. Song et al.[22] predicted that phase separation may or may not

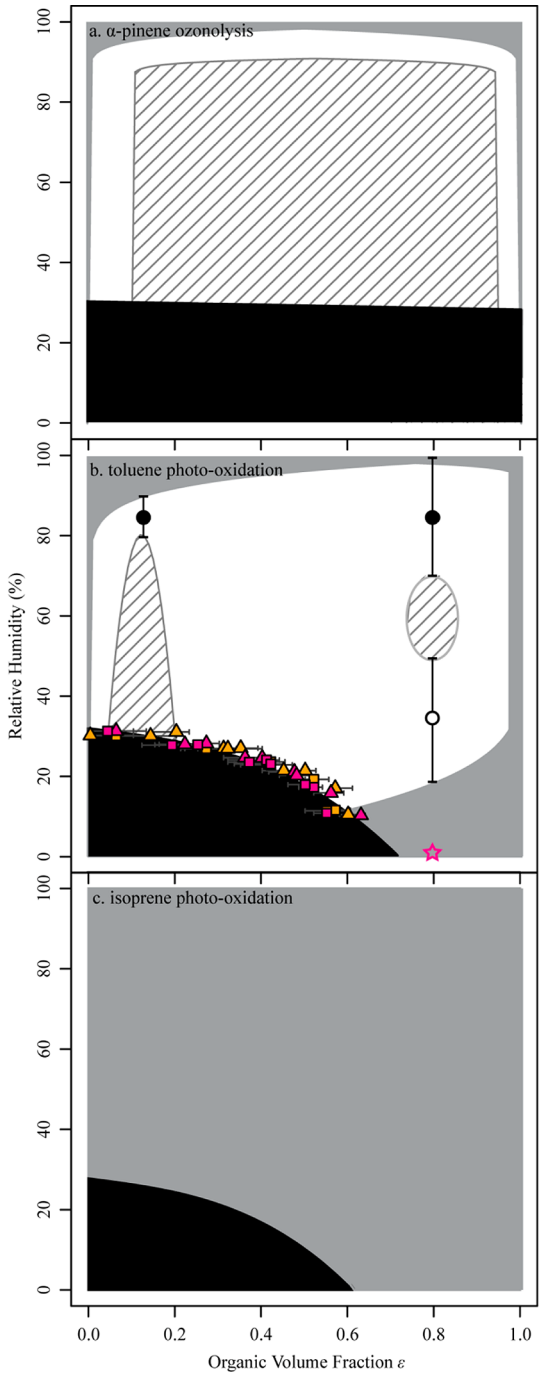


**Figure 6.** Phase diagrams highlighting miscibility regions for aqueous ammonium sulfate mixed with SOM produced by (a) $\alpha$-pinene ozonolysis, (b) toluene photo-oxidation, and (c) isoprene photo-oxidation. Diagrams are constructed based on data of Figures 4 and 5. Gray shading indicates regions in which the SOM and the aqueous salt are miscible. Gray hatching indicates regions of phase separation. Uncertainty in the boundaries between miscible and phase-separated regions, because of an absence of complete data, is conveyed by white space. Large portions of the miscible regions are metastable with respect to solid ammonium sulfate (i.e., RH < DRH($\varepsilon$)). Black coloring indicates effloresced regions. In panel b, the plotted circles designate the RH of phase separation derived from optical microscopy (Figure 5). Vertical error bars represent the range of observed SRH values from multiple experiments. ERH($\varepsilon$) data are reproduced from Figure 3.


dx.doi.org/10.1021/jp405095e | J. Phys. Chem. A 2013, 117, 8895−8906

occur, depending on the oxygen−carbon functional group composition of the organic material (for $0.56 \leq O/C \leq 0.8$). Both predictions indicating independence of phase separation organic volume fraction is again consistent with Figure 6. In the case of toluene-derived SOM, however, the representation in Figure 6 shows that the organic volume fraction must be taken into account when considering phase separation behavior. Bertram et al.[16] noted that phase separation can depend on the organic volume fraction (as expected from thermodynamic modeling of organic−inorganic phase diagrams[5,49]) and provided several data sets to that effect for pure compounds but omitted it in the parametrization because of the weak effect for the data sets studied.

The phase miscibility and phase transition properties of the components within mixed particles can influence their interactions with other components in the atmosphere. For example, organic coatings such as those observed for aqueous sulfate and SOM produced by $\alpha$-pinene ozonolysis can significantly reduce the uptake coefficient of reactive gases.[2,50] In the case of $N_2O_5$, the changed particle reactivity can in turn affect atmospheric concentrations of $NO_x$ and $O_3$.[4,24] Given the variability of properties observed for laboratory-generated SOM, different types of SOM-inorganic particles may influence the surrounding atmospheric environment through a number of different mechanisms that are not fully understood. These effects may differ over boreal forests associated with large quantities of terpene-derived SOM, tropical forests associated with large quantities of isoprene-derived SOM, and polluted megacities associated with large quantities of aromatic-derived SOM. However, a caution is that the properties of laboratory SOMs may differ from those of SOMs produced in the atmosphere. Therefore, further work is needed to investigate the variable phases of both laboratory-produced and atmospheric organic−inorganic particles, as well as the extent to which these phases and their particle morphologies affect the attendant atmospheric processes.

## ■ ASSOCIATED CONTENT

### Supporting Information

Measured and modeled number-diameter distributions for reference measurements, efflorescence tests, and deliquescence tests. Sensitivity analysis for $\varepsilon_D$ optimization. Description and results of the MCM-SIMPOL model. Additional microscopy images and movies collected by the microscopy technique. DRH($\varepsilon$) and ERH($\varepsilon$) data points and parametrizations. This material is available free of charge via the Internet at http://pubs.acs.org.

## ■ AUTHOR INFORMATION

### Corresponding Authors

*E-mail: scot_martin@harvard.edu (S.T.M.). Website: http://www.seas.harvard.edu/environmental-chemistry.
*E-mail: bertram@chem.ubc.ca (A.K.B.).

### Notes

The authors declare no competing financial interest.

## ■ ACKNOWLEDGMENTS

This research was supported by the National Science Foundation under Grant No. 0925467 and by the Office of Science, U.S. Department of Energy (S.T.M.). Any opinions, findings, and conclusions or recommendations expressed in this material are those of the authors and do not necessarily reflect the views of the National Science Foundation. Support is also gratefully acknowledged from the Natural Sciences and Engineering Research Council of Canada (NSERC) (A.K.B.). M.L.S. is the recipient of a Graduate Research Environmental Fellowship from the Global Change Education Program of the Department of Energy. A. Bateman is acknowledged for assistance and discussion during the chamber experiments. Y. Zhang provided the model simulations based on inclusion of the Master Chemical Mechanism for toluene into the model described in ref 37.

## ■ REFERENCES

(1) Seinfeld, J. H.; Pandis, S. N. *Atmospheric Chemistry and Physics: From Air Pollution to Climate Change*, 2nd ed.; Wiley: New York, 2006.
(2) Anttila, T.; Kiendler-Scharr, A.; Tillmann, R.; Mentel, T. F. On the Reactive Uptake of Gaseous Compounds by Organic-Coated Aqueous Aerosols: Theoretical Analysis and Application to the Heterogeneous Hydrolysis of $N_2O_5$. *J. Phys. Chem.* **2006**, *110*, 10435−10443.
(3) Martin, S. T.; Hung, H. M.; Park, R. J.; Jacob, D. J.; Spurr, R. J. D.; Chance, K. V.; Chin, M. Effects of the Physical State of Tropospheric Ammonium-Sulfate-Nitrate Particles on Global Aerosol Direct Radiative Forcing. *Atmos. Chem. Phys.* **2004**, *4*, 183−214.
(4) Riemer, N.; Vogel, H.; Vogel, B.; Anttila, T.; Kiendler-Scharr, A.; Mentel, T. F. Relative Importance of Organic Coatings for the Heterogeneous Hydrolysis of $N_2O_5$ During Summer in Europe. *J. Geophys. Res.* **2009**, *114*, D17307.
(5) Zuend, A.; Marcolli, C.; Peter, T.; Seinfeld, J. H. Computation of Liquid−Liquid Equilibria and Phase Stabilities: Implications for RH-Dependent Gas/Particle Partitioning of Organic−Inorganic Aerosols. *Atmos. Chem. Phys.* **2010**, *10*, 7795−7820.
(6) Hameri, K.; Vakeva, M.; Hansson, H. C.; Laaksonen, A. Hygroscopic Growth of Ultrafine Ammonium Sulphate Aerosol Measured Using an Ultrafine Tandem Differential Mobility Analyzer. *J. Geophys. Res.* **2000**, *105*, 22231−22242.
(7) Martin, S. T. Phase Transitions of Aqueous Atmospheric Particles. *Chem. Rev.* **2000**, *100*, 3403−3453.
(8) Tang, I. N.; Munkelwitz, H. R. An Investigation of Solute Nucleation in Levitated Solution Droplets. *J. Colloid Interface Sci.* **1984**, *98*, 430−438.
(9) Buzorius, G.; Zelenyuk, A.; Brechtel, F.; Imre, D. Simultaneous Determination of Individual Ambient Particle Size, Hygroscopicity and Composition. *Geophys. Res. Lett.* **2002**, *29*, 1974.
(10) Chen, S. C.; Tsai, C. J.; Chen, H. D.; Huang, C. Y.; Roam, G. D. The Influence of Relative Humidity on Nanoparticle Concentration and Particle Mass Distribution Measurements by the Moudi. *Aerosol Sci. Technol.* **2011**, *45*, 596−603.
(11) Murphy, D. M.; Cziczo, D. J.; Froyd, K. D.; Hudson, P. K.; Matthew, B. M.; Middlebrook, A. M.; Peltier, R. E.; Sullivan, A.; Thomson, D. S.; Weber, R. J. Single-Particle Mass Spectrometry of Tropospheric Aerosol Particles. *J. Geophys. Res.* **2006**, *111*, D23s32.
(12) Murphy, D. M.; Thomson, D. S.; Mahoney, T. M. J. In Situ Measurements of Organics, Meteoritic Material, Mercury, and Other Elements in Aerosols at 5 to 19 Kilometers. *Science* **1998**, *282*, 1664−1669.
(13) Pratt, K. A.; Prather, K. A. Aircraft Measurements of Vertical Profiles of Aerosol Mixing States. *J. Geophys. Res.* **2010**, *115*, D11305.
(14) Hallquist, M.; Wenger, J. C.; Baltensperger, U.; Rudich, Y.; Simpson, D.; Claeys, M.; Dommen, J.; Donahue, N. M.; George, C.; Goldstein, A. H.; et al. The Formation, Properties and Impact of Secondary Organic Aerosol: Current and Emerging Issues. *Atmos. Chem. Phys.* **2009**, *9*, 5155−5236.
(15) Ervens, B.; Turpin, B. J.; Weber, R. J. Secondary Organic Aerosol Formation in Cloud Droplets and Aqueous Particles (aqSOA): A Review of Laboratory, Field and Model Studies. *Atmos. Chem. Phys.* **2011**, *11*, 11069−11102.
(16) Bertram, A. K.; Martin, S. T.; Hanna, S. J.; Smith, M. L.; Bodsworth, A.; Chen, Q.; Kuwata, M.; Liu, A.; You, Y.; Zorn, S. R.

Predicting the Relative Humidities of Liquid−Liquid Phase Separation, Efflorescence, and Deliquescence of Mixed Particles of Ammonium Sulfate, Organic Material, and Water Using the Organic-to-Sulfate Mass Ratio of the Particle and the Oxygen-to-Carbon Elemental Ratio of the Organic Component. *Atmos. Chem. Phys.* **2011**, *11*, 10995−11006.
(17) Marcolli, C.; Krieger, U. K. Phase Changes During Hygroscopic Cycles of Mixed Organic/Inorganic Model Systems of Tropospheric Aerosols. *J. Phys. Chem.* **2006**, *110*, 1881−1893.
(18) Smith, M. L.; Bertram, A. K.; Martin, S. T. Deliquescence, Efflorescence, and Phase Miscibility of Mixed Particles of Ammonium Sulfate and Isoprene-Derived Secondary Organic Material. *Atmos. Chem. Phys.* **2012**, *12*, 9613−9628.
(19) Koop, T.; Bookhold, J.; Shiraiwa, M.; Poschl, U. Glass Transition and Phase State of Organic Compounds: Dependency on Molecular Properties and Implications for Secondary Organic Aerosols in the Atmosphere. *Phys. Chem. Chem. Phys.* **2011**, *13*, 19238−19255.
(20) Smith, M. L.; Kuwata, M.; Martin, S. T. Secondary Organic Material Produced by the Dark Ozonolysis of α-Pinene Minimally Affects the Deliquescence and Efflorescence of Ammonium Sulfate. *Aerosol Sci. Technol.* **2011**, *45*, 244−261.
(21) Ciobanu, V. G.; Marcolli, C.; Krieger, U. K.; Weers, U.; Peter, T. Liquid−Liquid Phase Separation in Mixed Organic/Inorganic Aerosol Particles. *J. Phys. Chem.* **2009**, *113*, 10966−10978.
(22) Song, M.; Marcolli, C.; Krieger, U. K.; Zuend, A.; Peter, T. Liquid−Liquid Phase Separation in Aerosol Particles: Dependence on O:C, Organic Functionalities, and Compositional Complexity. *Geophys. Res. Lett.* **2012**, *39*, L19801.
(23) Takahama, S.; Pathak, R. K.; Pandis, S. N. Efflorescence Transitions of Ammonium Sulfate Particles Coated with Secondary Organic Aerosol. *Environ. Sci. Technol.* **2007**, *41*, 2289−2295.
(24) You, Y.; Renbaum-Wolff, L.; Carreras-Sospedra, M.; Hanna, S. J.; Hiranuma, N.; Kamal, S.; Smith, M. L.; Zhang, X.; Weber, R. J.; Shilling, J. E.; et al. Images Reveal That Atmospheric Particles Can Undergo Liquid−Liquid Phase Separations. *Proc. Natl. Acad. Sci. U.S.A.* **2012**, *109*, 13188−13193.
(25) Saathoff, H.; Naumann, K. H.; Schnaiter, M.; Schock, W.; Mohler, O.; Schurath, U.; Weingartner, E.; Gysel, M.; Baltensperger, U. Coating of Soot and $(NH_4)_2SO_4$ Particles by Ozonolysis Products of α-Pinene. *J. Aerosol Sci.* **2003**, *34*, 1297−1321.
(26) Meyer, N. K.; Duplissy, J.; Gysel, M.; Metzger, A.; Dommen, J.; Weingartner, E.; Alfarra, M. R.; Prevot, A. S. H.; Fletcher, C.; Good, N.; et al. Analysis of the Hygroscopic and Volatile Properties of Ammonium Sulphate Seeded and Unseeded SOA Particles. *Atmos. Chem. Phys.* **2009**, *9*, 721−732.
(27) Kleindienst, T. E.; Smith, D. F.; Li, W.; Edney, E. O.; Driscoll, D. J.; Speer, R. E.; Weathers, W. S. Secondary Organic Aerosol Formation from the Oxidation of Aromatic Hydrocarbons in the Presence of Dry Submicron Ammonium Sulfate Aerosol. *Atmos. Environ.* **1999**, *33*, 3669−3681.
(28) Shilling, J. E.; Chen, Q.; King, S. M.; Rosenoern, T.; Kroll, J. H.; Worsnop, D. R.; DeCarlo, P. F.; Aiken, A. C.; Sueper, D.; Jimenez, J. L.; et al. Loading-Dependent Elemental Composition of α-Pinene SOA Particles. *Atmos. Chem. Phys.* **2009**, *9*, 771−782.
(29) Tsigaridis, K.; Kanakidou, M. Global Modelling of Secondary Organic Aerosol in the Troposphere: A Sensitivity Analysis. *Atmos. Chem. Phys.* **2003**, *3*, 1849−1869.
(30) Henze, D. K.; Seinfeld, J. H.; Ng, N. L.; Kroll, J. H.; Fu, T. M.; Jacob, D. J.; Heald, C. L. Global Modeling of Secondary Organic Aerosol Formation from Aromatic Hydrocarbons: High- vs. Low-Yield Pathways. *Atmos. Chem. Phys.* **2008**, *8*, 2405−2420.
(31) Duplissy, J.; Gysel, M.; Sjogren, S.; Meyer, N.; Good, N.; Kammermann, L.; Michaud, V.; Weigel, R.; dos Santos, S. M.; Gruening, C.; et al. Intercomparison Study of Six HTDMAs: Results and Recommendations. *Atmos. Meas. Tech.* **2009**, *2*, 363−378.
(32) King, S. M.; Rosenoern, T.; Shilling, J. E.; Chen, Q.; Martin, S. T. Increased Cloud Activation Potential of Secondary Organic Aerosol for Atmospheric Mass Loadings. *Atmos. Chem. Phys.* **2009**, *9*, 2959−2971.
(33) Shilling, J. E.; Chen, Q.; King, S. M.; Rosenoern, T.; Kroll, J. H.; Worsnop, D. R.; McKinney, K. A.; Martin, S. T. Particle Mass Yield in Secondary Organic Aerosol Formed by the Dark Ozonolysis of α-Pinene. *Atmos. Chem. Phys.* **2008**, *8*, 2073−2088.
(34) Kuwata, M.; Martin, S. T. Particle Size Distributions Following Condensational Growth in Continuous Flow Aerosol Reactors as Derived from Residence Time Distributions: Theoretical Development and Application to Secondary Organic Aerosol. *Aerosol Sci. Technol.* **2012**, *46*, 937−949.
(35) Aiken, A. C.; DeCarlo, P. F.; Jimenez, J. L. Elemental Analysis of Organic Species with Electron Ionization High-Resolution Mass Spectrometry. *Anal. Chem.* **2007**, *79*, 8350−8358.
(36) Jenkin, M. E.; Saunders, S. M.; Wagner, V.; Pilling, M. J. Protocol for the Development of the Master Chemical Mechanism, MCM V3 (Part B): Tropospheric Degradation of Aromatic Volatile Organic Compounds. *Atmos. Chem. Phys.* **2003**, *3*, 181−193.
(37) Chen, Q.; Liu, Y.; Donahue, N. M.; Shilling, J. E.; Martin, S. T. Particle-Phase Chemistry of Secondary Organic Material: Modeled Compared to Measured O:C and H:C Elemental Ratios Provide Constraints. *Environ. Sci. Technol.* **2011**, *45*, 4763−4770.
(38) Gysel, M.; McFiggans, G. B.; Coe, H. Inversion of Tandem Differential Mobility Analyser (TDMA) Measurements. *J. Aerosol Sci.* **2009**, *40*, 134−151.
(39) Liu, B. Y. H.; Pui, D. Y. H.; Whitby, K. T.; Kittelson, D. B.; Kousaka, Y.; McKenzie, R. L. The Aerosol Mobility Chromatograph: A New Detector for Sulfuric Acid Aerosols. *Atmos. Environ.* **1978**, *12*, 99−104.
(40) Nakao, S.; Tang, P.; Tang, X.; Clark, C. H.; Qi, L.; Seo, E.; Asa-Awuku, A.; Cocker, D., III. Density and Elemental Ratios of Secondary Organic Aerosol: Application of a Density Prediction Method. *Atmos. Environ.* **2013**, *68*, 273−277.
(41) Biskos, G.; Paulsen, D.; Russell, L. M.; Buseck, P. R.; Martin, S. T. Prompt Deliquescence and Efflorescence of Aerosol Nanoparticles. *Atmos. Chem. Phys.* **2006**, *6*, 4633−4642.
(42) Berry, R. S.; Rice, S. A.; Ross, J. *Physical Chemistry*, 2nd ed.; Oxford University Press: New York, 2000.
(43) Song, M.; Marcolli, C.; Krieger, U. K.; Peter, T. Liquid−Liquid Phase Separation and Morphology of Internally Mixed Dicarboxylic Acids/Ammonium Sulfate/Water Particles. *Atmos. Chem. Phys.* **2012**, *12*, 2691−2712.
(44) Krieger, U. K.; Marcolli, C.; Reid, J. P. Exploring the Complexity of Aerosol Particle Properties and Processes Using Single Particle Techniques. *Chem. Soc. Rev.* **2012**, *41*, 6631−6662.
(45) Anttila, T.; Kiendler-Scharr, A.; Mentel, T. F.; Tillmann, R. Size Dependent Partitioning of Organic Material: Evidence for the Formation of Organic Coatings on Aqueous Aerosols. *J. Atmos. Chem.* **2007**, *57*, 215−237.
(46) Prisle, N. L.; Engelhart, G. J.; Bilde, M.; Donahue, N. M. Humidity Influence on Gas-Particle Phase Partitioning of α-Pinene + $O_3$ Secondary Organic Aerosol. *Geophys. Res. Lett.* **2010**, 37.
(47) Pant, A.; Parsons, M. T.; Bertram, A. K. Crystallization of Aqueous Ammonium Sulfate Particles Internally Mixed with Soot and Kaolinite: Crystallization Relative Humidities and Nucleation Rates. *J. Phys. Chem.* **2006**, *110*, 8701−8709.
(48) Parsons, M. T.; Riffell, J. L.; Bertram, A. K. Crystallization of Aqueous Inorganic-Malonic Acid Particles: Nucleation Rates, Dependence on Size, and Dependence on the Ammonium-to-Sulfate. *J. Phys. Chem.* **2006**, *110*, 8108−8115.
(49) Zuend, A.; Seinfeld, J. H. A Practical Method for the Calculation of Liquid−Liquid Equilibria in Multicomponent Organic−Water−Electrolyte Systems Using Physicochemical Constraints. *Fluid Phase Equilib.* **2013**, *337*, 201−213.
(50) Folkers, M.; Mentel, T. F.; Wahner, A. Influence of an Organic Coating on the Reactivity of Aqueous Aerosols Probed by the Heterogeneous Hydrolysis of $N_2O_5$. *Geophys. Res. Lett.* **2003**, *30*, 1644.